HAL
open science

Controlling the properties of PbTiO 3 / SrTiO 3 superlattices by photoexcited carriers

Carmel Dansou, Charles Paillard, Laurent Bellaiche

To cite this version:

Carmel Dansou, Charles Paillard, Laurent Bellaiche. Controlling the properties of PbTiO 3 / SrTiO 3 superlattices by photoexcited carriers. Physical Review B, 2022, 106 (22), pp.L220101. 10.1103/PhysRevB.106.L220101 . hal-03899818

HAL Id: hal-03899818

https://centralesupelec.hal.science/hal-03899818v1

Submitted on 15 Dec 2022

HAL is a multi-disciplinary open access archive for the deposit and dissemination of scientific research documents, whether they are published or not. The documents may come from teaching and research institutions in France or abroad, or from public or private research centers.

L'archive ouverte pluridisciplinaire **HAL**, est destinée au dépôt et à la diffusion de documents scientifiques de niveau recherche, publiés ou non, émanant des établissements d'enseignement et de recherche français ou étrangers, des laboratoires publics ou privés.

Controlling properties of $PbTiO_3/SrTiO_3$ superlattices by photo-excited carriers

Carmel Dansou[1], Charles Paillard[2], and Laurent Bellaiche[1]
[1] *University of Arkansas, Fayetteville, Arkansas 72701, USA and*
[2] *Laboratoire SPMS, CentraleSupélec/CNRS, UNR 8580, Université Paris-Saclay, 91190 Gif-sur-Yvette, France*
(Dated: November 30, 2022)

The effect of light on properties of $PbTiO_3/SrTiO_3$ superlattices is studied using first-principles calculations in their paraelectric phase p as well as in the, c, r and aa phases that are defined by polarization lying along [001], [11v] and [110] directions, respectively. Whilst the r phase is the ground state in dark conditions, illumination triggers a rotation of the polarization towards the out-of-plane direction, which results in the r phase transforming into a c phase at large concentration of photoexcited carriers. We further reveal that a space charge region of free carriers builds up at the interface under illumination, implying that these superlattices can be thought as acting as p-i-n junctions under light. These free charges screen the polarization discontinuity at the interface, effectively reducing the electrostatic depolarizing field.

I. INTRODUCTION

$(PbTiO_3/SrTiO_3)_m$ superlattices ($(PTO/STO)_m$ SLs) have gained a lot of attention [1–11]. It was found that, by turning the epitaxial strain and the PTO volume fraction, a large variety of fascinating properties can be engineered in these SLs [1, 2, 4]. They have, e.g., been found to host non trivial topological structures [7–10] and negative capacitance [12], which are of fundamental as well as practical interest [13].

There have also been significant developments in the interaction of light with ferroelectric (FE) materials during the last decade [14, 15], with light having the capability to induce structural change (photostriction) and even phase transition in classical FE materials [14, 16, 19–21]. More recently it was also reported that one can control the topology of phonons in FE materials with light [18].

It is now natural and timely to ask whether light can modulate physical properties of FE SLs. For example, it was reported that under illumination, PTO/STO SLs transform from a polydomain structure to a uniform domain configuration [22]. This transition was accompanied by the expansion of the out-of-plane lattice of the SLs. A light-induced polarization rotation was also evidenced at the nanoscale in multidomains [23], as well as an optically-induced phase transition from a vortex and domain state to a so-called super crystal phase in PTO/STO SLs [24]. However, light interaction with FE SLs, has been mostly experimentally studied so far. To the best of our knowledge, theoretical investigations were limited to phenomenologically varying the dielectric constant of the dielectric layer to reproduce the super crystal phase [24]. Microscopic insights are thus lacking. Many questions remain unresolved, such as what are the microscopic mechanisms favoring photo-induced transitions in these SLs or change in their physical properties under light.

Here, we explore light interaction with monodomain $(PbTiO_3/SrTiO_3)_m$ SLs. Technically, we apply our recently developed scheme to mimic the effect of photo-induced thermalized carriers [17] on the relative energy and phase stability of different phases having different electrical polarization orientation. We observe photo-induced phase transitions and change in properties, and further reveal their microscopic origins via the development of an analytical model demonstrating that these SLs can be thought as p-i-n junctions when under illumination.

II. METHODS

A. Constraint density functional theory

The constraint density functional theory (c-DFT) is a purpose built method to simulate photo-excitation in pump-probe optical experiment within the known DFT framework. Photo-excited thermalized electrons and holes are described using Fermi-Dirac distribution with two chemical potentials, μ_e for electrons and μ_h for holes. During the self consistent field DFT cycles, the electronic density is converged with the constraint of having $n_e = n_{ph}$ electrons per formula unit in the conduction band and $n_h = n_{ph}$ holes in the valence band. Explicitly one solves numerically for the couple of chemical potentials $(\mu_e,\ \mu_h)$ using the following equations at each SCF cycle:

$$n_h = \sum_{i \leq N_v} \sum_{k,\sigma} w_k \left[1 - f\left(\epsilon_{ik,\sigma}, \mu_h\right)\right] \tag{1}$$

$$n_e = \sum_{i > N_v} \sum_{k,\sigma} w_k f\left(\epsilon_{ik,\sigma}, \mu_e\right) \tag{2}$$

w_k is the weight of the k-point $\mathbf{k}$, $f\left(\epsilon_{ik,\sigma}\right)$ is the occupation number, σ stands for spin and N_v is the index of highest occupied band [17]. This scheme recently implemented in the Abinit package has proven to successfully mimic the effects of photo-excited carriers in ferroelectrics [17].

B. Computational details

We performed density functional theory (DFT) calculations as implemented in the Abinit package [25] with the projector augmented wave method [26]. The generalized gradient approximation with the Perdew-Burke-Ernzerhof parameterization revised for solid was used as the exchange-correlation functional [27]. A 20 Ha plane wave cut-off was employed in our calculations. A $6\times6\times1$ k-meshes equivalent to a $6\times6\times6$ mesh in a five-atom unit cell allows to reach convergency for both forces and energies. Density was considered converged when the difference of forces on atoms between two self-consistent field iterations is less that 1×10^{-7} Ha.Bohr^{-1}. Both cell shape and ionic positions were further optimized until the maximum forces on the ions were less than 2×10^{-5} Ha.Bohr^{-1}.

We simulated monodomains in $(PTO)_5/(STO)_5$ SLs that are built by stacking along the [001] direction five unit cells of PTO and five unit cells of STO. The choice of a 5/5 PTO/STO SLs as a model for this study is inspired by previous studies and our computational resources. When simulating light interaction with the superlattices, calculations become very heavy for larger supercells. As such we had to choose the size of the superlattices to be thick enough but in accordance with the resource's constraints. Also, a 5/5 PTO/STO film has been experimentally grown [11], which demonstrates the experimental relevance of our choice. The in-plane lattice constant was kept fixed at the theoretical optimized lattice constant of STO, in order to mimic a growth on a STO substrate. First, the SLs were optimized to find a reference paraelectric structure with mirror symmetry called the p phase [28]. Three other phases are then considered: the c phase with a polarization along the out-of-plane [001] direction; the aa phase with a polarization lying along the in-plane [110] direction; and the r phase with a polarization being along [uuv] directions [28]. Starting from the optimized structure under dark conditions, light-interaction with these phases was then simulated using the c-DFT. When under light, both cell shape and ions positions of the structures were again relaxed with the aforementioned parameters.

III. RESULTS

A. Energy and stability

On Figure 1 , we show the relative energies of the different phases (with respect to the p reference phase) for various excited charged carriers concentration (n_{ph}). In dark condition ($n_{ph}=0$ electron per formula unit (e/f.u)), the most stable phase is the r phase where the polarization points along a specific [11v] direction, such that it makes an angle $\theta\approx72°$ with the z-axis. As we increase the light intensity (n_{ph}), the relative energy of the c phase gets closer to that of the r phase until the two basically coincide for n_{ph} larger than 0.2 e/f.u. As we will see later, such behaviors originate from the facts that, under light, the r phase first rotates its polarization towards the [001] direction and then transforms into the c phase that becomes the ground state. Meanwhile, the energy of the aa phase increases away from its ground state's energy, as n_{ph} increases.

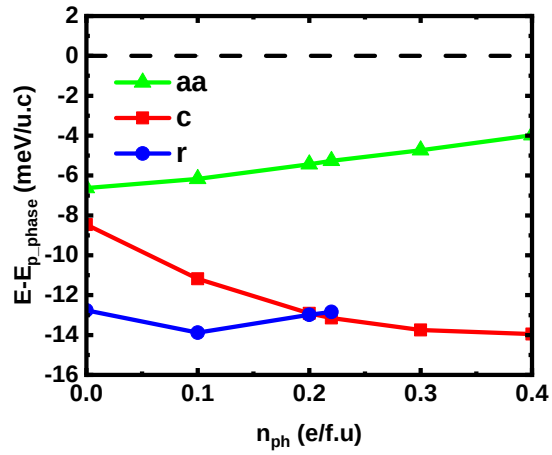

FIG. 1. Relative energies of the different phases. The zero of energy is chosen to be that of the p phase, for any illumination.

B. Light-induced polarization and lattice dynamism in the c phase

To further determine effects of light on the different phases, we also compute the polarization in layer-by-layer fashion using the Born effective charges of the atoms in each local unit cell via:

$$P_i=\frac{e}{\Omega_i}\sum_{j\in i}w_j\delta_j Z_j^* \tag{3}$$

where Ω_i, e, and δ_j are the volume of the unit cell i, the elementary charge and the atomic displacement from the reference paraelectric p phase, respectively. Z_j^* is the Born effective charge of the atom j, with j running through all the atoms in the cell i and w_j being a weight corresponding to the number of five-atoms unit cell that share the atom j. The Born charges Z_j^* are taken from Refs. [29].

The data are shown in Figure 2 (a) for the c phase. In dark condition, the electrical polarization throughout the SLs is nearly constant, as consistent with previous reports [30, 31] and which arises from the minimization of the electrostatic cost associated with bound charges at the interfaces. Under illumination, the electrical polarization in PTO layers increases while the polarization in STO layers decreases. The polarization in the interfacial regions (unit cells 5 and 10 on Figure 2 (a)) remains

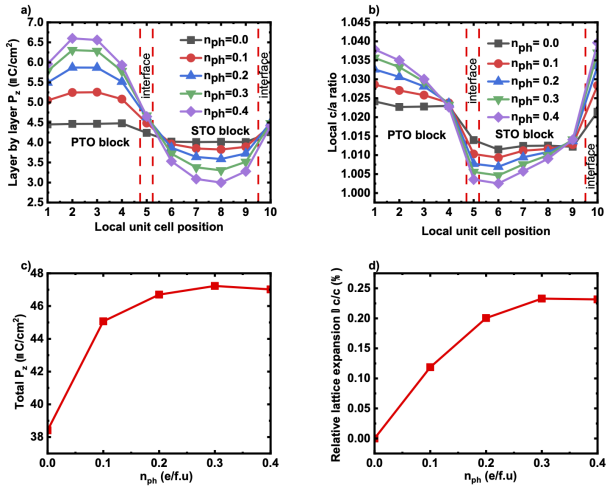

FIG. 2. Layer-by-layer polarization (a), local out-of-plane lattice distortion (b), total polarization (c) and relative lattice expansion in the c phase.

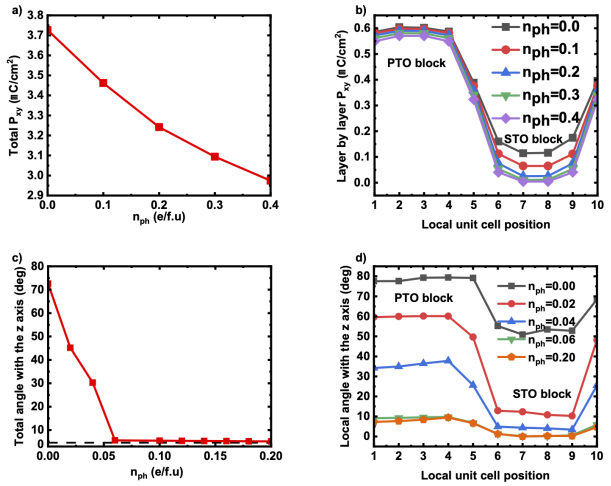

FIG. 3. Total in plane polarization (a) and local polarization (b) in the aa phase; angle of the electrical polarization with the z-axis in the r phase: a) global angle, b) local angle.

mainly unaffected. The overall polarization, however, increases with light intensity, as shown in Figure 2 (c). The increase of the polarization in the SLs is accompanied by an increase in local out-of-plane lattice distortion in PTO layers as well as in global out-of-plane lattice of the SLs, as revealed by Figures 2 (b) and (d) and as also found in optical excitation experiment on PTO/STO SLs having multidomains [22]. The local out-of-plane distortion is quantified as $(z^i_{A_2} - z^i_{A_1})/a$ where $z^i_{A_1}$, $z^i_{A_2}$ are the z-positions of the $A_{j=1,2}$ = Pb or Sr atoms at the corners of the cell i in the SLs with $z^i_{A_1} < z^i_{A_2}$; and a is the in-plane lattice constant of the SLs.

C. Light-induced polarization dynamism in the aa phase

We also looked at the *aa* phase and the effect of light on its polarization. On Figures 3 (a&b), we show the total and local in-plane polarizations of this *aa* phase, as function of light intensity. The total electrical polarization of the aa phase decreases with n_{ph}, indicating that light penalizes in-plane polar displacements. This finding is also consistent with the steady increase in the energy of this *aa* phase seen in Fig. 1. Furthermore, inspection of the layer-by-layer polarization in the *aa* phase, as shown on Figure 3 (b), indicates that the decrease of its polarization mostly comes from the STO layers that tend to become paraelectric under light (in dark condition, the STO layers are ferroelectric as a consequence of their proximity with PTO layers within our considered supercell).

D. Light-induced polarization rotation in the r phase

The observations from the *c* and *aa* phases imply that in the *r* phase, the in-plane component of the electrical polarization should be reduced while its out-of plane component should be increased by illumination. This should thus lead to the polarization in the *r* phase rotating towards the out-of-plane direction upon illumination, and to the transition from the *r* to the *c* phase observed in the energy diagram on Figure 1. We map out the angle between the z-axis and the electrical polarization within the *r* phase as function of n_{ph}. The results shown on Figs. 3 (c &d) are well consistent with our above explanations. We therefore have a light-induced polarization rotation within the *r* phase. Similar light-induced polarization rotation has been seen at domain boundaries in multidomain PTO/STO SLs where the polarization rotates from an *r*-like orientation to a *c*-like orientation upon optical excitation [23], in-line with our predictions. In Fig. 3 (d), we show the variation of the angle of the polarization with the z axis across the SLs. Under illumination, the polarization in the STO layer rotates faster towards the z axis and this angle is almost zero for all value of $n_{ph} > 0.06$ e/f.u which indicates that, beyond a certain light intensity, the polarization in the STO layer stays practically along the z axis. Any further rotation of the polarization in the SLs beyond $n_{ph} > 0.06$ e/f.u, therefore, emanates mostly from the rotation of the local polarization in the PTO layers.

E. Light-induced depolarization field screening

Next, we look at the macro-averaged [32, 33] (also detailed in Ref.[34], Sec. 1) electrostatic potential

and charges density inside the c phase as function of n_{ph}. From the macro-averaged potential, we deduce the macro-averaged internal electric field by numerical finite difference differentiation of the potential data with respect to z [35]. In dark condition and as shown in Figure 4(a) via the blue curve, there is a finite electric field in both PTO and STO layers, consistent with previous reports on FE-dielectrics SLs [30, 36], with short-circuit boundary conditions requiring the fields in the PTO and STO layers to be opposite in sign. It is the polarization mismatch between PTO and STO layers that induces this electric field in the STO layer [37, 38]. These internal fields act as depolarizing fields limiting the polarization in the SLs. As we photo-excite charged carriers, they

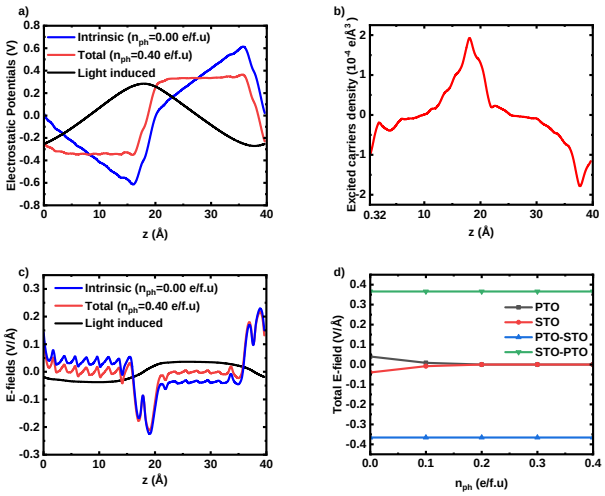

FIG. 4. The different potentials for $n_{ph} = 0.4$ e/f.u and $n_{ph} = 0$ e/f.u; b) the difference of the macroscopic average excited charged carriers density between the case of $n_{ph} = 0.4$ e/f.u and $n_{ph} = 0$ e/f.u; c) E-fields for $n_{ph} = 0.4$ e/f.u and $n_{ph} = 0$ e/f.u; d) total E-field in different part of the Sls as a function of light intensity.

mainly populate the interface regions of the PTO/STO SLs as evidenced by the difference, shown in Fig. 4 (b), in the macroscopic average in the charged carriers density between one illumination ($n_{ph} = 0.4$ e/f.u) and dark conditions (the same trend is obtained for other values of n_{ph}). Interfaces are populated by opposite but equal amount of excited charged carriers. Our results agree with some existing experimental reports indicating that excited charges carriers migrate to the interfaces to screen the depolarizing field [22, 23]. However, for the considered SLs thickness, the excited charged carriers are rather significantly localized at the interfaces while they tail into PTO and STO layers. This feature has been observed in previous studies on electron gas at $LaAlO_3/SrTiO_3$ where for thin film, the free gas was observed to also tail into the STO layers [39, 40]. Consequently, the internal electric fields in PTO and STO layers reduce their value under illumination (see the red curve *versus* the blue curve in Figure 4 (c)) and even quench for n_{ph} equal or larger than 0.2 e/f.u – as revealed by Fig. 4 (d). For each considered finite n_{ph}, one can also define a light-induced potential that consists of the difference between the total electrostatic potential for such finite n_{ph} and the one for $n_{ph} = 0$, as shown via black solid lines in Figure 4 (a). Such light-induced potential can be understood as a light-induced electric field (see Figure 4 (c) for the case of $n_{ph} = 0.4$ e/f.u.). In both PTO and STO layers, light produces fields opposite to the intrinsic internal field leading to a net zero field in these layers (Figure 4 (c)). We therefore have a light-induced depolarizing field screening. In contrast, light has very negligible effect on the fields at the two interfaces, as demonstrated in both Figures 4 (c) and 4 (d).

F. Electro-static model of light-induced dynamism

In the following, we propose a simple electrostatic model to account for the light-induced change in electrostatics in the SLs. For simplicity, we assume that the excited charged carriers are significantly localized and homogeneously populate the interface regions, and that PTO and STO are mainly recombination regions where there is no net excited charged carriers. In one unit cell of the SLs, the volume charge density of excited carriers can be defined as follows:

$$\rho^l(z) = \begin{cases} 0, \ z_0 \leq z \ \leq z_1 \\ +\rho_v, \ z_1 \leq z \ \leq z_2 \\ 0, \ z_2 \leq z \ \leq z_3 \\ -\rho_v, \ z_3 \leq z \ \leq z_4 \end{cases} , \rho_v = \frac{\int_{z_1}^{z_2} \rho(z) dz}{z_2 - z_1}. \quad (4)$$

where $\rho(z)$ are the difference in the macro-averaged charged density (see, e.g., Fig. 4 (b) for the case of ($n_{ph} = 0.4$ e/f.u); z_0 and z_1 the boundaries of the PTO layer; z_1 and z_2 the boundaries of PTO-STO interface; z_2 and z_3 the boundaries of the STO layer and z_3 and z_4 those of the STO-PTO interface. The values of z_1, z_2, z_3, z_4 are extracted from our computational data and are $(z_0, z_1, z_2, z_3, z_4) \approx (0.32, 16.10, 20.06, 35.84, 39.63)$ Å. The above-defined charge density is similar to charges density in a typical p-i-n junction in semiconductors [41–43]. Using basic electrostatic equations:

$$\frac{dE^l(z)}{dz} = -\frac{d^2V^l(z)}{dz^2} = \frac{\rho_v}{\epsilon}. \quad (5)$$

where ϵ is the static permittivity which value changes throughout the SLs, i.e $\epsilon = \epsilon_{PTO}$ in the PTO layer, $\epsilon = \epsilon_{STO}$ in the STO layer, and the average of the dielectric permitivities of PTO and STO is taken as an approximation of ϵ at the interfaces. Note, however, that we did not use any previously computed values of ϵ but rather extracted the ratio $\rho_v/\epsilon \approx 0.02$ V.Å^{-2} from the slope of the computed light-induced field in the interface regions (Figure 4 (c)). The light-induced electrostatic field and potential are as follows:

$$E^l(z) = \begin{cases} -E_0^l, \ z_0 \leq z \ \leq z_1 \\ -E_0^l + \dfrac{z - z_1}{\epsilon}\rho_v, \ z_1 \leq z \ \leq z_2 \\ +E_0^l, \ z_2 \leq z \ \leq z_3 \\ E_0^l - \dfrac{z - z_3}{\epsilon}\rho_v, \ z_3 \leq z \ \leq z_4 \end{cases} \quad ; \ V^l(z) = \begin{cases} (z - z_0)E_0^l + V_0, \ z_0 \leq z \ \leq z_1 \\ V_1^l + (z - z_1)E_0^l - \dfrac{(z - z_1)^2}{2\epsilon}\rho_v, \ z_1 \leq z \ \leq z_2 \\ V_2^l - (z - z_2)E_0^l, \ z_2 \leq z \ \leq z_3 \\ V_3^l + (z_3 - z)E_0^l + \dfrac{(z - z_3)^2}{2\epsilon}\rho_v, \ z_3 \leq z \ \leq z_4 \end{cases} \tag{6}$$

with $E_0^l \approx 0.036$ V.Å^{-1} being the strength of the light-induced field at $z_0 = 0.32$ Å and $(V_0^l, V_1^l, V_2^l, V_3^l) \approx (-0.26, 0.26, 0.26, -0.26)$ V being the electrostatic potentials induced by light at z_0, z_1, z_2, z_3 respectively – as extracted from DFT data plotted on Figs. 4 (a&b). On Figure 5, we show the results of our analytical model and compared them with the data from our DFT computations for the highest studied light intensity ($n_{ph} = 0.4$ e/f.u). The agreement is rather good for both the light-induced field and electrostatic potential. One can then conclude that, at the microscopic level, illuminated PTO/STO SLs act like p-i-n junctions with (1) the PTO-STO interface being the p-region; (2) the STO-PTO interface being the n-region; and (3) PTO and STO layers being the i-regions (intrinsic zone of neutral charges sandwiched between the p and n regions). The photo-induced electric fields produced by this (p-i-n)-like junction in PTO and STO layers screen out the depolarization field inside the PTO and STO layers. The supplemental material reports the results of another model that is similar in spirit with the one described by equation (4) (that is, excited charged carriers are strongly localized at the interfaces) but with different form for $\rho(z)$ (See Ref.[34], Sec. 2).

IV. DISCUSSION

Here we would like to point to some existing models proposed in literature to produce screening layer at PTO/STO interface by turning PTO films thickness [44–46]. In those models, the free carriers can only be produced when the electrical polarization is normal to the interface. As such, one cannot use these models to study the impact of free carriers on the electrical polarization in the aa and the r phases considered in our study.

Also, we did not consider oxygen octahedral rotation or tilting in this work that are are known to compete with polarization in some systems. This is mostly because we first wanted to know the effect of light on polarization alone in the studied superlattices but also because neither PTO nor STO possesses such rotation or tilting at room temperature (which is the temperature at which measurements are typically done). The effect of excited charged carriers on these antiferrodistortive modes and their coupling with polarization in these SLs, as well as the additional effect of varying the epitaxial strain, are interesting questions to explore for future studies.

Finally, note that in the present study, we limit ourselves to monodomains in these SLs in order to first reveal and understand the impact of photoexcitation on different polar phases before tackling the more complex impact of light on polydomains. The extension of this study to polydomain SLs is left for future exploration.

V. CONCLUSION

In summary, we report a first-principle investigation of the impact of light on energetic and physical properties of monodomain $(PTO)_5/(STO)_5$ SLs. From energetics and electrostatic analysis, we now understand that the polarization in close to open-circuit conditions will grow under illumination as photo-excited carriers will screen the polarization bound charges. On the other hand, the polarization in directions close to short-circuit conditions reduces under illumination, as reminiscent of results in bulk ferroelectrics [16]. In our specific case, this results in the polarization rotation of the r phase of monodomain PTO/STO SLs towards that of the c phase under illumination. The favoring of an out-of-plane polarization under illumination thus helps explaining the transition to a monodomain state observed in Ref.[22] or the domain boundary rotation discussed in Ref.[23]. We therefore hope that the present study deepens the active field of light-matter interaction and can be used to design novel efficient devices using light as a physical handle since, e.g., rotation of polarization is known to dramatically enhance many physical properties, including piezoelectricity, dielectric responses as well as elasto-optical and electro-optical conversions [47–50].

ACKNOWLEDGMENTS

The work is supported by the ARO Grants No. W911NF-21-2-0162 (ETHOS) and W911NF-21-1-0113, and the Vannevar Bush Faculty Fellowship (VBFF) grant no. N00014-20-1-2834 from the Department of Defense. C.P. thanks the support from a public grant overseen by the French National Research Agency (ANR) as part of the "Investissements d'Avenir" program (Labex NanoSaclay, reference: ANR-10-LABX-0035).

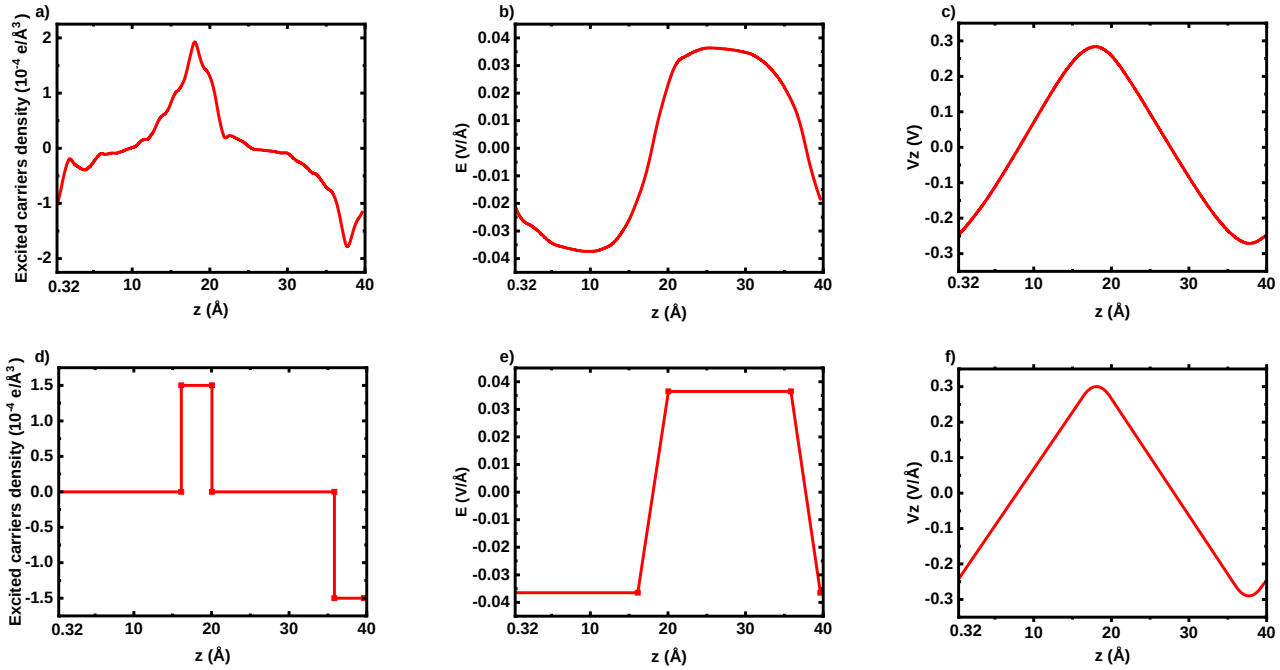

FIG. 5. Comparison between the DFT data (first row) and the presently developed analytical model (second row) about light-induced electrostatics for the case of $n_{ph} = 0.4$ e/f.u. a) and d) correspond to difference in the macro-averaged charged density, b) and e) represent the light-induced electric field, c) and f) correspond to the light-induced electrostatic potential.

[1] M. Dawber, C. Lichtensteiger, M. Cantoni, M. Veithen, P. Ghosez, K. Johnston, K. M. Rabe, J. M. Triscone, Unusual behavior of the Ferroelectric polarization in $PbTiO_3/SrTiO_3$ superlattices, Phys. Rev. Lett. **95**, 177601 (2005).

[2] M. Dawber, N. Stucki, C. Lichtensteiger, S. Gariglio, P. Ghosez, J. M. Triscone, Tailoring the properties of artificially layered ferroelectric superlattices, Adv. Mater. **19**, 4153 (2007).

[3] P. Aguado-Puente, P. Garcia-Fernandez, J. Junquera, Interplay of couplings between antiferrodistortive, ferroelectric, and strain degrees of freedom in monodomain $PbTiO_3/SrTiO_3$ superlattices, Phys. Rev. Lett. **107**, 217601 (2011).

[4] E. Bousquet, M. Dawber, N. Stucki, C. Lichtensteiger, P. Hermet, S. Gariglio, J. M. Triscone, P. Ghosez, Improper ferroelectricity in perovskite oxide artificial superlattices, Nature **452**, 732 (2008).

[5] I. Misirlioglu, M. Alexe, L. Pintilie, D. Hesse, Space charge contribution to the apparent enhancement of polarization in ferroelectric bilayers and multilayers, Appl. Phys. Lett. **91**, 022911 (2007).

[6] V. R. Cooper, K. Johnston, K. M. Rabe, Polarization enhancement in short period superlattices via interfacial intermixing, Phys. Rev. B **76**, 020103(R) (2007).

[7] S. Das, Y. Tang, Z. Hong, M. Gonçalves, M. McCarter, C. Klewe, K. Nguyen, F. Gómez-Ortiz, P. Shafer, E. Arenholz, V. A. Stoica, S. L. Hsu, B. Wang, C. Ophus, J. F. Liu, C. T. Nelson, S. Saremi, B. Prasad, A. B. Mei, D. G. Schlom, J. Íñiguez, P. García-Fernández, D. A. Muller, L. Q. Chen, J. Junquera, L. W. Martin, R. Ramesh, Observation of room-temperature polar skyrmions, Nature **568**, 368, (2019).

[8] A. Yadav, C. Nelson, S. Hsu, Z. Hong, J. Clarkson, C. Schlepütz, A. Damodaran, P. Shafer, E. Arenholz, L. Dedon, D. Chen, A. Vishwanath, A. M. Minor, L. Q. Chen, J. F. Scott, L. W. Martin, R. Ramesh, Observation of polar vortices in oxide superlattices, Nature **530**, 198, (2016).

[9] A. Y. Abid, Y. Sun, X. Hou, C. Tan, X. Zhong, R. Zhu, H. Chen, K. Qu, Y. Li, M. Wu, J. Zhang, J. Wang, K. Liu, X. Bai, D. Yu, X. Ouyang, J. Wang, J. Li, P. Gao, Creating polar antivortex in $PbTiO_3/SrTiO_3$ superlattice, Nature Commun. **12**, 1 (2021).

[10] P. Aguado-Puente, J. Junquera, Structural and energetic properties of domains in $PbTiO_3/SrTiO_3$ superlattices from first principles, Phys. Rev. B **85**, 184105 (2012).

[11] P. Zubko, N. Jecklin, N. Stucki, C. Lichtensteiger, G. Rispens, J. M. Triscone, Ferroelectric Domains in $PbTiO_3/SrTiO_3$ superlattices, Ferroelectrics **433**, 127 (2012).

[12] P. Zubko, J. C. Wojdeł, M. Hadjimichael, S. Fernandez-Pena, A. Sené, I. Luk'yanchuk, J. M. Triscone, J. Íñiguez, Negative capacitance in multidomain ferroelectric superlattices, Nature **534**, 524 (2016).

[13] S. Das, Z. Hong, M. McCarter, P. Shafer, Y. T. Shao, D. Muller, L. Martin, R. Ramesh, A new era in ferroelectrics, APL Mater. **8**, 120902 (2020).

[14] B. Kundys, Photostrictive materials, Appl. Phys. Rev. **2**, 011301 (2015).

[15] C. Paillard, X. Bai, I. C. Infante, M. Guennou, G. Geneste, M. Alexe, J. Kreisel, B. Dkhil, Photovoltaics with Ferroelectrics: Current Status and Beyond, Adv. Mater. **28**, 5153 (2016).

[16] C. Paillard, B. Xu, B. Dkhil, G. Geneste, L. Bellaiche, Photostriction in ferroelectrics from density functional theory, Phys. Rev. Lett. **116**, 247401 (2016).

[17] C. Paillard, E. Torun, L. Wirtz, J. Íñiguez, L. Bellaiche, Photoinduced phase transitions in ferroelectrics, Phys. Rev. Lett. **123**, 087601 (2019).

[18] B. Peng, Y. Hu, S. Murakami, T. Zhang, B. Monserrat, Topological phonons in oxide perovskites controlled by light, Science Adv. **6**, 1618 (2020).

[19] P. Chen, C. Paillard, H. J. Zhao, J. Íñiguez, L. Bellaiche, Deterministic control of ferroelectric polarization by ultrafast laser pulses, Nature Commun. **13**, 2566 (2022).

[20] R. Haleoot, C. Paillard, T. P. Kaloni, M. Mehboudi, B. Xu, L. Bellaiche, S. Barraza-Lopez, Photostrictive Two-Dimensional Materials in the Monochalcogenide Family, Phys. Rev. Lett. **118**, 227401 (2017).

[21] C. Paillard, S. Prosandeev, L. Bellaiche, Ab initio approach to photostriction in classical ferroelectric materials, Phys. Rev. B **96**, 045205 (2017).

[22] Y. Ahn, J. Park, A. Pateras, M. B. Rich, Q. Zhang, P. Chen, M. H. Yusuf, H. Wen, M. Dawber, P. G. Evans, Photoinduced domain pattern transformation in ferroelectric-dielectric superlattices, Phys. Rev. Lett. **119**, 057601 (2017).

[23] H. J. Lee, Y. Ahn, S. D. Marks, E. C. Landahl, S. Zhuang, M. H. Yusuf, M. Dawber, J. Y. Lee, T. Y. Kim, S. Unithrattil, S. H. Chun, S. Kim, I. Eom, S. Y. Park , K. S. Kim, S. Lee, J. Y. Jo, J. Hu, P. G. Evans, Structural evidence for ultrafast polarization rotation in ferroelectric/dielectric superlattice nanodomains, Phys. Rev. X **11**, 031031 (2021).

[24] V. Stoica, N. Laanait, C. Dai, Z. Hong, Y. Yuan, Z. Zhang, S. Lei, M. McCarter, A. Yadav, A. Damodaran, S. Das, G. A. Stone, J. Karapetrova, D. A. Walko, X. Zhang, L. W. Martin, R. Ramesh, L. Q. Chen, H. Wen, V. Gopalan, J. W. Freeland, Optical creation of a supercrystal with three-dimensional nanoscale periodicity, Nature Mater. **18**, 377 (2019).

[25] A. H. Romero, D. C. Allan, B. Amadon, G. Antonius, T. Applencourt, L. Baguet, J. Bieder, F. Bottin, J. Bouchet, E. Bousquet, F. Bruneval, G. Brunin, D. Caliste, M. Coté, J. Denier, C. Dreyer, P. Ghosez, M. Giantomassi, Y. Gillet, O. Gingras, D. R. Hamann, G. Hautier, F. Jollet, G. Jonard, A. Martin H. P. C. Miranda, F. Naccarato, G. Petretto, N. A. Pike, V. Planes, S. Prokhorenko, T. Rangel, F. Ricci, G. M. Rignanese, M. Royo, M. Stengel, M. Torrent, M. J. van Setten, B. Van Troeye, M. J. Verstraete, J. Wiktor, J. W. Zwanziger, X. Gonze, Abinit: Overview and focus on selected capabilities, J. Chem. Phys. **152**, 124102 (2020).

[26] M. Torrent, F. Jollet, F. Bottin, G. Zérah, X. Gonze, Implementation of the projector augmented-wave method in the ABINIT code: Application to the study of iron under pressure, Comput. Mat. Science **42**, 337 (2008).

[27] J. P. Perdew, A. Ruzsinszky, G. I. Csonka, O. A. Vydrov, G. E. Scuseria, L. A. Constantin, X. Zhou, K. Burke, Restoring the Density-Gradient Expansion for Exchange in Solids and Surfaces, Phys. Rev. Lett. **100**, 136406 (2008).

[28] N. Pertsev, A. Zembilgotov, A. Tagantsev, Effect of mechanical boundary conditions on phase diagrams of epitaxial ferroelectric thin films, Phys. Rev. Lett. **80**, 1988 (1998).

[29] W. Zhong, R. D. King-Smith, D. Vanderbilt, Giant LO-TO splittings in perovskite ferroelectrics, Phys. Rev. Lett. **72**, 3618 (1994).

[30] J. B. Neaton, K. M. Rabe, Theory of polarization enhancement in epitaxial $BaTiO_3/SrTiO_3$ superlattices, Appl. Phys. Lett. **82**, 1586, (2003).

[31] Z. Zhu, B. Wang, H. Wang, Y. Zheng, Q. Li, First-principle study of ferroelectricity in $PbTiO_3/SrTiO_3$ superlattices, Solid-state electronics **50**, 1756 (2006).

[32] J. Junquera, M. H. Cohen, K. M. Rabe, Nanoscale smoothing and the analysis of interfacial charge and dipolar densities, J. Phys: Cond. Mat. **19**, 213203 (2007).

[33] A. Baldereschi, S. Baroni, R. Resta, Band Offsets in Lattice-Matched Heterojunctions: A Model and First-Principles Calculations for GaAs/AlAs, Phys. Rev. Lett. **61**, 734 (1988)

[34] See supplemental materials at [URL] for details on the macro-averaging procedure as implemented in Abinit (section 1) and for another electrostatic model (section 2).

[35] Q. Kong, T. Siauw, A. Bayen, *Python Programming and Numerical Methods: A Guide for Engineers and Scientists*, Academic Press, **2020**.

[36] M. Sepliarsky, S. R. Phillpot, D. Wolf, M. G. Stachiotti, R. L. Migoni, Long-ranged ferroelectric interactions in perovskite superlattices, Phys. Rev. B **64**, 060101(R) (2001).

[37] K. G. Lim, K. H. Chew, L. H. Ong, M. Iwata, Electrostatic coupling and interface intermixing in ferroelectric superlattices, Europhys. Lett. **99**, 46004 (2012).

[38] A. L. Roytburd, S. Zhong, S. P. Alpay, Dielectric anomaly due to electrostatic coupling in ferroelectric-paraelectric bilayers and multilayers, Appl. Phys. Lett. **87**, 092902 (2005).

[39] P. Delugas, A. Filippetti, V. Fiorentini, Spontaneous 2-Dimensional Carrier Confinement at the n-Type $SrTiO_3/LaAlO_3$ interface, Phys. Rev. Lett. **106**, 166807 (2011).

[40] M. Stengel, First-Principles Modeling of Electrostatically Doped Perovskite Systems, Phys. Rev. Lett. **106**, 136803 (2011).

[41] F. Berz, A simplified theory of the p-i-n diode, Solid-State Electronics **20**, 709 (1977).

[42] B. G. Streetman, S. Banerjee, *Solid state electronic devices*, Pearson/Prentice Hall Upper Saddle River, USA, **2006**.

[43] B. J. Baliga, *Fundamentals of power semiconductor devices*, Springer, USA, **2010**.

[44] P. Aguado-Puente, N. C. Bristowe, B. Yin, R. Shirasawa, P. Ghosez, P. B. Littlewood, E. Artacho, Model of two-dimensional electron gas formation at ferroelectric interfaces, Phys. Rev B **92**, 035438 (2015).

[45] B. Yin, P. Aguado-Puente, S. Qu, E. Artacho, Two-dimensional electron gas at the $PbTiO_3/SrTiO_3$ interface: An ab initio study, Phys. Rev B **92**, 115406 (2015).

[46] E. A. Eliseev, S. V. Kalinin, A. N. Morozovska, J. Appl. Phys. **117**, 034102 (2015).

[47] L. Bellaiche, A. García, D. Vanderbilt, Finite-temperature properties of $PbZr_{(1-x)}Ti_xO_3$ alloys from first principles, Phys. Rev. Lett. **84**, 5427 (2000).

[48] L. Bellaiche, A. García, D. Vanderbilt, Low-temperature properties of $PbZr_{(1-x)}Ti_xO_3$ solid solutions near the morphotropic phase boundary, Ferroelectrics **266**, 41 (2002).

[49] L. Chen, Y. Yang, Z. Gui, D. Sando, M. Bibes, X. K. Meng, L. Bellaiche, Large elasto-optic effect in epitaxial $PbTiO_3$ films, Phys. Rev. Lett. **115**, 267602 (2015).

[50] C. Paillard, S. Prokhorenko, L. Bellaiche, Strain engineering of electro-optic constants in ferroelectric materials, npj Comput. Mater. **5**, 1 (2019).